

Proceeding Paper

Testing the Drop-Size Distribution Based Separation of Stratiform and Convective Rain Using Radar and Disdrometer Data from a Midlatitude Coastal Region [†]

Merhala Thurai ^{1,*}, Viswanathan Bringi ¹, David Wolff ², David Marks ^{2,3} and Charanjit Pabla ^{2,3}

¹ Department of Electrical and Computer Engineering, Colorado State University, Fort Collins, CO 80523, USA; bringi@engr.colostate.edu

² NASA GSFC Wallops Flight Facility, Wallops Island, VA 23337, USA; david.b.wolff@nasa.gov (D.W.); david.a.marks@nasa.gov (D.M.); charanjit.s.pabla@nasa.gov (C.P.)

³ Science Systems and Applications, Inc., Lanham, MD 20706, USA

* Correspondence: merhala@colostate.edu; Tel.: +1-970-491-7678

[†] Presented at the 3rd International Electronic Conference on Atmospheric Sciences, 16–30 November 2020; Available online: <https://ecas2020.sciforum.net/>.

Abstract: Stratiform and convective rain are associated with different microphysical processes and generally produce drop-size distributions (DSDs) with different characteristics. A previous study, using data from a tropical coastal location found that the two rain types could be separated in the N_w – D_m space, where D_m is the mass-weighted mean diameter and N_w is the normalized intercept parameter. The separation method has also been tested using data and observations from a mid-latitude continental location with semiarid climate, and a subtropical continental location. In this paper, we investigate the same separation technique using data and observations from a midlatitude coastal region. Three-minute DSDs from disdrometer measurements were used for the N_w versus D_m based classification and were compared with simultaneous observations from an S-band polarimetric radar 38 km away from the disdrometer site. Specifically, range-height indicator (RHI) scans over the disdrometer were used for confirmation. The results showed that there was no need to modify the separation criteria from previous studies. Scattering calculations using the three-minute DSDs were used to derive retrieval equations for N_w and D_m for the S-band radar and applied to the RHI scans to identify convective and stratiform rain regions. Two events are shown as illustrative examples.

Keywords: stratiform rain; convective rain; raindrop-size distributions; polarimetric radar retrievals

Citation: Thurai, M.; Bringi, V.; Wolff, D.; Marks, D.; Pabla, C. Testing the Drop-Size Distribution Based Separation of Stratiform and Convective Rain Using Radar and Disdrometer Data from a Mid-Latitude Coastal Region. *Proceedings* **2021**, *4*, 13. <https://doi.org/10.3390/ecas2020-08125>

Academic Editor: Anthony R. Lupu

Published: 13 November 2020

Publisher's Note: MDPI stays neutral with regard to jurisdictional claims in published maps and institutional affiliations.



Copyright: © 2020 by the authors. Licensee MDPI, Basel, Switzerland. This article is an open access article distributed under the terms and conditions of the Creative Commons Attribution (CC BY) license (<http://creativecommons.org/licenses/by/4.0/>).

1. Introduction

The importance of classification of rain types as convective and stratiform is related to the very different microphysical processes that go into the formation of their respective drop-size distributions (DSDs). It is well known (e.g., [1]) that stratiform rain is defined by large areas of weak vertical air motion, with the dominant feature being the reflectivity bright-band where snow aggregates (falling slowly at ~1 m/s) melt to rain, whereas convective rain forms from melting graupel and hail in compact reflectivity “cells” within strong downdrafts. This leads to different methods of estimating rain rates for hydrology, as well as calculating the latent heating (vertical) profiles in the stratiform and convective rain areas [2]. Houze [3] has clearly shown the impact of the latent heating profiles on precipitation evolution. Furthermore, while the stratiform rain rates are typically <10 mm/h, their large areal extent and long duration (e.g., outer rain bands of hurricanes) relative to convective rain make the classification an important topic of

study.

Differences in drop-size distributions (DSDs) between stratiform and convective rain have also been examined in the past by several researchers, e.g., [4,5], and [6], who used ground-based disdrometer data, as well as [7–9], and [10], who used aircraft data (from particle-imaging probes). More recently, Bukovcic et al. [11] used DSD data from a 2D video disdrometer (2DVD: [12,13]) in central Oklahoma, USA to separate stratiform and convective rain by applying a multivariable Bayesian classification algorithm, whereas Bringi et al. [14] used dual-polarized radar, dual-frequency profilers, and ground-based Joss–Waldvogel disdrometer data to investigate the use of two main parameters governing the DSD characteristics for the separation. Specifically, they found that the two rain types could be separated in the N_w – D_m space, where D_m is the mass-weighted mean diameter and N_w is the normalized intercept parameter. The data used in that study (see also [15]) were obtained from Darwin, Australia, which is a tropical oceanic location. Since then, the separation technique has been tested using data and observations from Huntsville, Alabama, USA, [16] a subtropical continental location, as well as Greeley, Colorado, USA, [17], a midlatitude continental location with semiarid climate. For the Huntsville events, 2DVD data were used for the separation method, and validation was provided by simultaneous observations from an ultra-high frequency (UHF) Doppler profiler collocated with the 2DVD. For the Greeley events, composited DSD data from 2DVD and an optical array probe called the Meteorological Particle Spectrometer (MPS: [18–20]) were used, and validation was provided by range-height indicator (RHI) scans by an S-band polarimetric radar (named CSU-CHILL radar, [21]) over the ground-based instruments.

In this paper, we investigate the same separation technique using data and observations from a midlatitude coastal region, situated in the Delmarva peninsula in Virginia. As with the Greeley cases, measurements from a 2DVD and an MPS were used to construct the full DSD spectra and the N_w versus D_m based separation is compared with simultaneous observations from an S-band polarimetric radar located 38 km away from the disdrometer site. Three-minute DSDs are used for the classification, and RHI radar scans over the disdrometer are used for testing. Three very different rain events are considered.

2. Instrumentation and Observations

2.1. DSD

The instrumentation location belongs to the NASA Wallops Flight Facility (WFF) and is part of the ground-validation activities in support of the Global Precipitation Measurement (GPM) Mission [22], as well as studies on precipitation microphysics, e.g., [23]. The ground instruments included many different types of disdrometers and rain gauges, including an MPS, several 2DVDs and a Pluvio rain gauge [24], all collocated at the same coastal site. The MPS and one of the 2DVD units was installed within a 2/3rd-scaled double wind fence (DFIR; [25]) to reduce the effects of high winds on the measurements of small drops. The MPS was used for relatively accurate measurements of drop concentration of small drops (<1 mm drop diameter), and the 2DVD provided more accurate measurements for the larger diameters, i.e., >1 mm. The composite or the full DSD was then constructed using the MPS and the 2DVD measurements over a three-minute time interval. The overlap region has been investigated before [26]; that study found that the best agreement between the two instruments was obtained in the diameter range of 0.75–1 mm.

2.2. Radar Observations

The polarimetric radar used for confirmation in this study was the NASA Polarimetric (NPOL) radar [27] located NNE of the disdrometer site, as shown in Figure 1. The azimuth of the disdrometers (shown in orange) from the radar was 197°. The radar scan

strategy included volume scans; RHI scans with azimuths of 195° , 197° , and 199° ; and, for Z_{dr} calibration, 90° elevation “birdbath” scans. This sequence was repeated regularly, every 7 min and 15 s. RHI scans along the 197° azimuth were chosen for classifying stratiform or convective rain in this study. Specifically, vertical profiles of reflectivity (Z_h), differential reflectivity (Z_{dr}), and copolar correlation coefficient (ρ_{hv}) were extracted over the disdrometer site to establish whether the melting layer could be clearly distinguished well above the ground level.

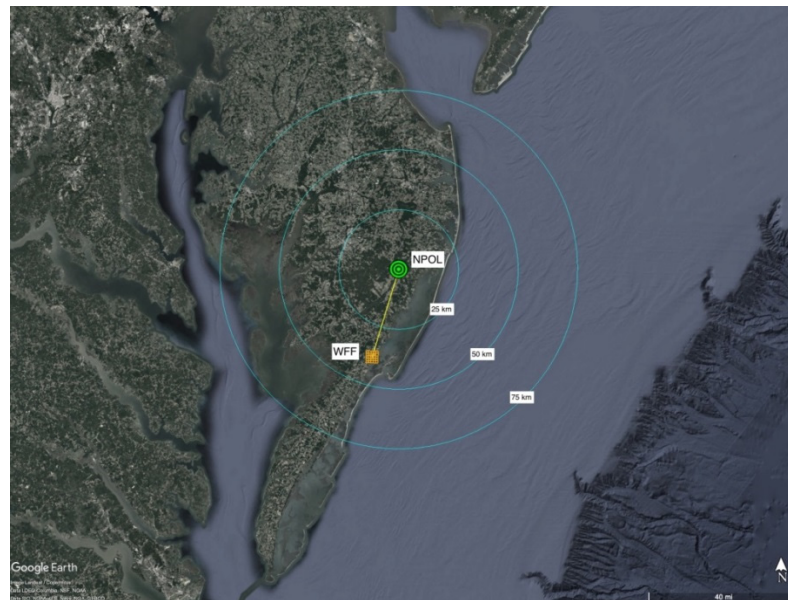


Figure 1. NPOL radar and the disdrometer location.

2.3. Rain Events

We considered three events here: (i) a category-1 hurricane event (Dorian), whose rainbands passed over the WFF site on 6 September 2019 ([28,29]); (ii) a squall-line event with a not so well-organized line convection that occurred on 14 October 2019; and (iii) a more widespread event with small embedded convective cells that occurred on 16 October 2019.

For all cases, the NPOL radar had performed the regular routine scans. Figure 2 shows two examples of RHI scans over the disdrometer, one on the 16th of October (Z_h in panel (a) and Z_{dr} in panel (b)) and the other on the 14th of October 2019 (Z_h in panel (c) and Z_{dr} in panel (d)). The top two panels show stratiform rain over the disdrometer site (which is marked with vertical black lines), indicated by the clear presence of radar bright-band caused by the melting layer between 3 and 3.5 km height above ground level (a.g.l.). The melting layer is visible in both Z_h and Z_{dr} . By contrast, panels (c) and (d) do not show any radar bright-band in the entire RHI scan, thus it can be classified as convective rain. Panels (e) and (f) show the 1-minute composite DSDs measured by the disdrometers at the same times as panels (a)/(b) and (c)/(d), respectively. For the latter, larger drops can be seen, with maximum recorded diameter (equi-volume drop diameter, D_{eq}) of nearly 4 mm, whereas for the former it was just over 3 mm.

Two further examples are given in Figure 3. Panels (a) and (b) correspond to the Dorian rain-band event on 6 September 2019, showing very clear bright-band between 4 and 4.5 km a.g.l., and panels (c) and (d) show another convective rain example that occurred on 14 October 2019. Once again, the black lines indicate the location of and over the disdrometers. Vertical profiles of Z_h and ρ_{hv} over the disdrometer site for the stratiform rain case (panels (a)/(b)) are shown in panels (e) and (f), and those for the convective rain case (panels (c)/(d)) are shown in panels (g) and (h). In all cases, vertical profiles were extracted over a 37 to 39 km range interval.

Clear differences are seen: (i) the Z_h profile for the stratiform rain in Figure 3 show very clear peak at around 4 km height, unlike the convective rain, where the Z_h profiles are “noisy” and do not show any clearly defined features; (ii) the ρ_{hv} profiles show a “dip” just below the melting layer in panel (e) for the stratiform rain, whereas the convective rain profiles in panel (h) show an almost constant ρ_{hv} of 0.99. Such features were used to identify (or classify) the two rain types.

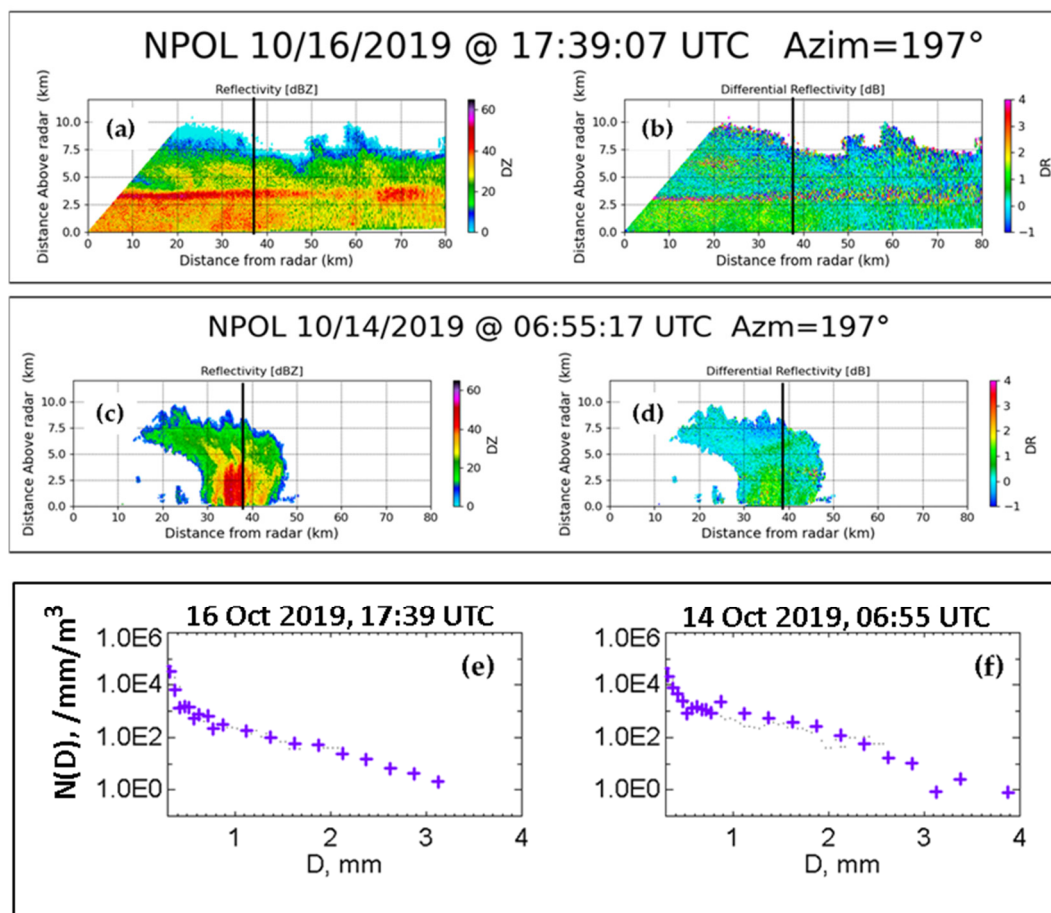


Figure 2. RHI scans of (a) Z_h and (b) Z_{dr} during a stratiform rain event on 16 October 2019; (c) and (d): RHI scans of Z_h and Z_{dr} , respectively, during a convective rain event on 14 October 2019; (e) 1-min composite DSD from disdrometers for case (a); (f) 1-min DSD for case (c). The vertical black lines in the RHI scan correspond to the range of (and height above) the disdrometers.

3. N_w Versus D_m Variations

The 1-min DSDs for the four cases in Figures 2 and 3 were used to derive the DSD moments, and from there, the parameters N_w and D_m were calculated using well-established formulas; e.g., [28] and [26]. They are shown as “+” points in Figure 4 and marked with the figure number corresponding to the four events. The red dashed line represents the stratiform-convective rain separation line from the previous studies [14–16]. The points for Figures 2a and 3a lie below the separation line, and hence were categorized as stratiform rain, and those for Figures 2c and 3c lie above the separation line, and thus were categorized as convective rain. These were indeed consistent with the radar observations for all four events.

In our previous studies, a simple “index” parameter i (empirically-derived) also was used to indicate whether the N_w versus D_m lay above or below the separation line. Stratiform rain is indicated by i when it is negative, and convective rain is indicated by i when it is positive. The same procedure was used here. The index values (derived from 3-min

DSD based N_w-D_m for the 14 October 2019 are shown in Figure 5 for the whole duration of the event. The separation line (i.e., $i = 0$) is also included. As seen, there were several cases with positive i or i close to 0. These are numbered from (i) through (vii). The corresponding RHI scans from NPOL are given in Figure 6. In all cases, the arrows point to the precipitation structure above the disdrometers.

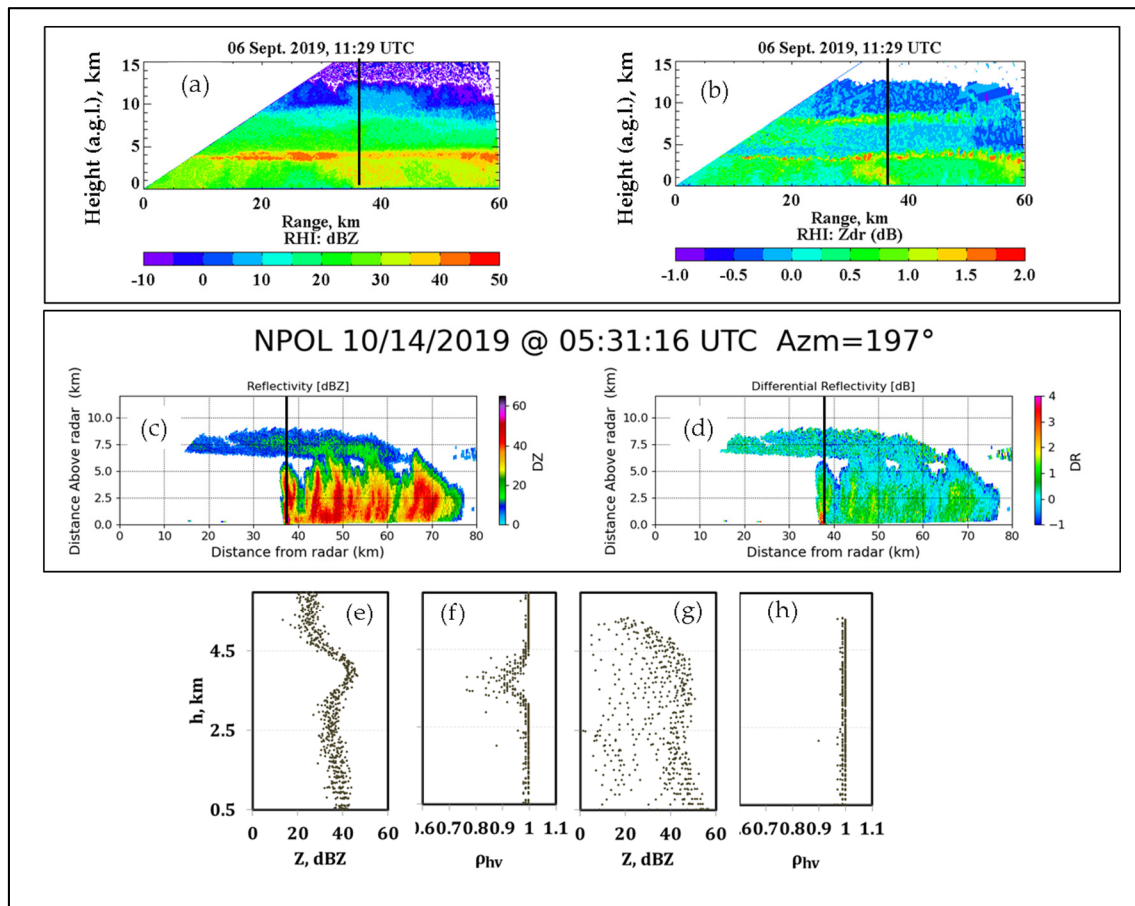


Figure 3. RHI scans of (a) Z_h and (b) Z_{dr} during a stratiform rain event on 6 September 2019 (rain-bands of Dorian storm); (c) and (d): RHI scans of Z_h and Z_{dr} , respectively, during another convective rain event on 14 October 2019; (e) and (f): vertical profiles of Z_h and ρ_{hv} , respectively, over the disdrometers for case (a); (g) and (h): vertical profiles of Z_h and ρ_{hv} , respectively, over the disdrometers for case (c).

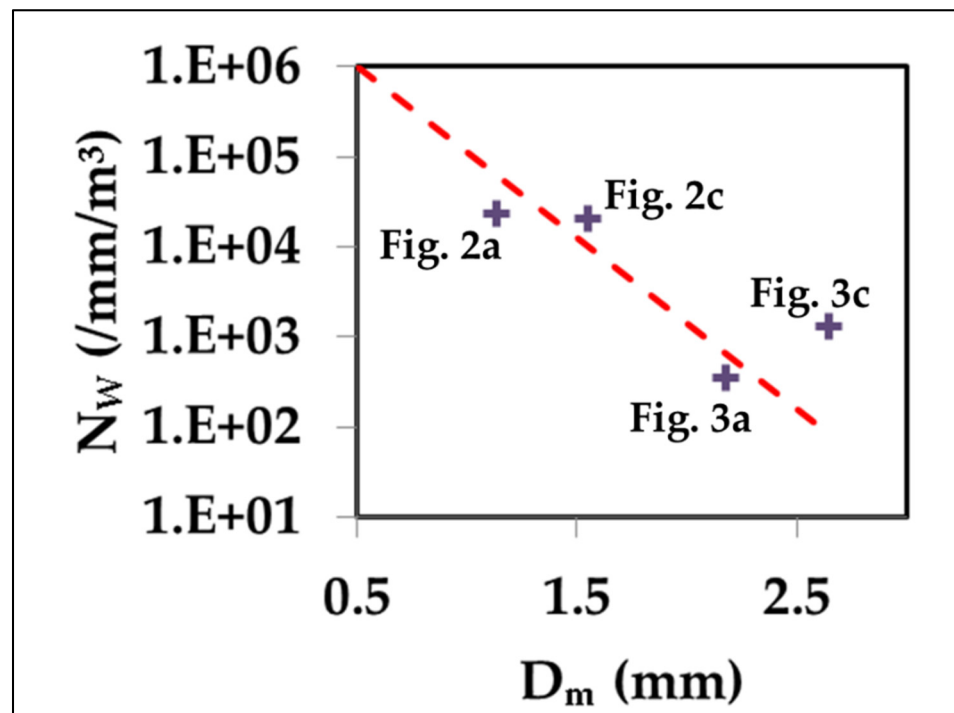


Figure 4. N_w versus D_m from 1 or 3 min DSDs corresponding to Figures 2a,c and 3a,d, as marked.

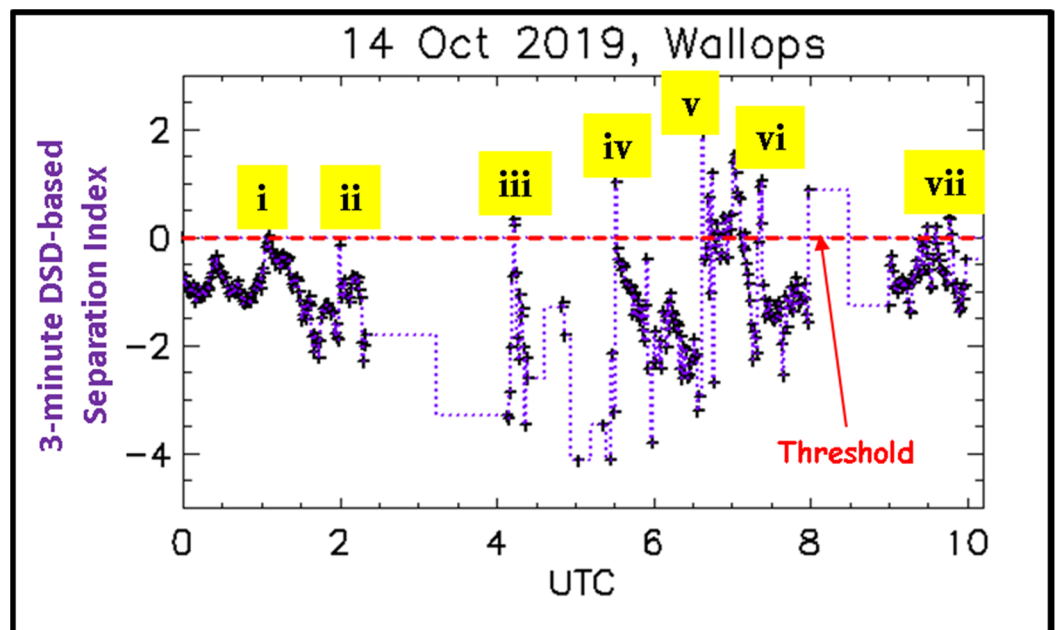


Figure 5. Variation of the “index” parameter with time for the 14 October 2019 event. Cases (i) to (vii) are marked where the index reaches close to or above the 0 threshold.

Cases (i) and (ii) had relatively thick bright-bands, and from Figure 5 we see that the index values approached zero. By comparison, in [16], DSD and profiler data during a “cold-rain” event in Ontario, Canada, showed that the index i became closer to zero with bright-band peak values within the melting layer in stratiform rain. Given that thicker bright-bands have higher dBZ peaks, cases (i) and (ii) in Figure 6 appear to be consistent with the results from the Ontario event.

Case (iii) from Figure 6 shows convective rain over the disdrometer site, but relatively moderate in intensity and limited in its size, that is, its core spanned less than 5 km in range. For this case, the index lay just above the red line.

Cases (iv), (v), and (vi) were more typical of convective rain, but the strong echoes, unlike deep convection, did not reach very high heights. Nevertheless, the index values were significantly above the zero threshold.

Case (vii) can be categorized as shallow convection (from last panel of Figure 6), with echo tops being below 5 km a.g.l. For this case, the index lay just above zero. D_m values during this period were lower than those during cases (iv), (v), and (vi) (not shown here).

Next, we considered the event on 16 October 2019. This too lasted for several hours, and the index values based on 3 min DSDs are shown in Figure 7. They went above the zero threshold only at around 17:00 UTC. Three time periods are marked: (i), the index was well below zero; (ii), was slightly above zero; and (iii), was negative but close to zero.

The corresponding NPOL RHI scans are given in Figure 8. Case (i) did not show a clear bright-band in dBZ, but the Z_{dr} plot showed the enhancement more clearly. The RHI scan from case (ii) appeared to indicate modest convection over the disdrometer site, although the Z_{dr} plot showed enhancement beyond the 40 km range. One could classify this case as “mixed” or “transition”. Case (iii) was a thick bright-band case, with high dBZ peak in the melting layer (>50 dBZ). The index value at this time was very similar to case (i) of the 14 October event shown earlier in Figures 5 and 6.

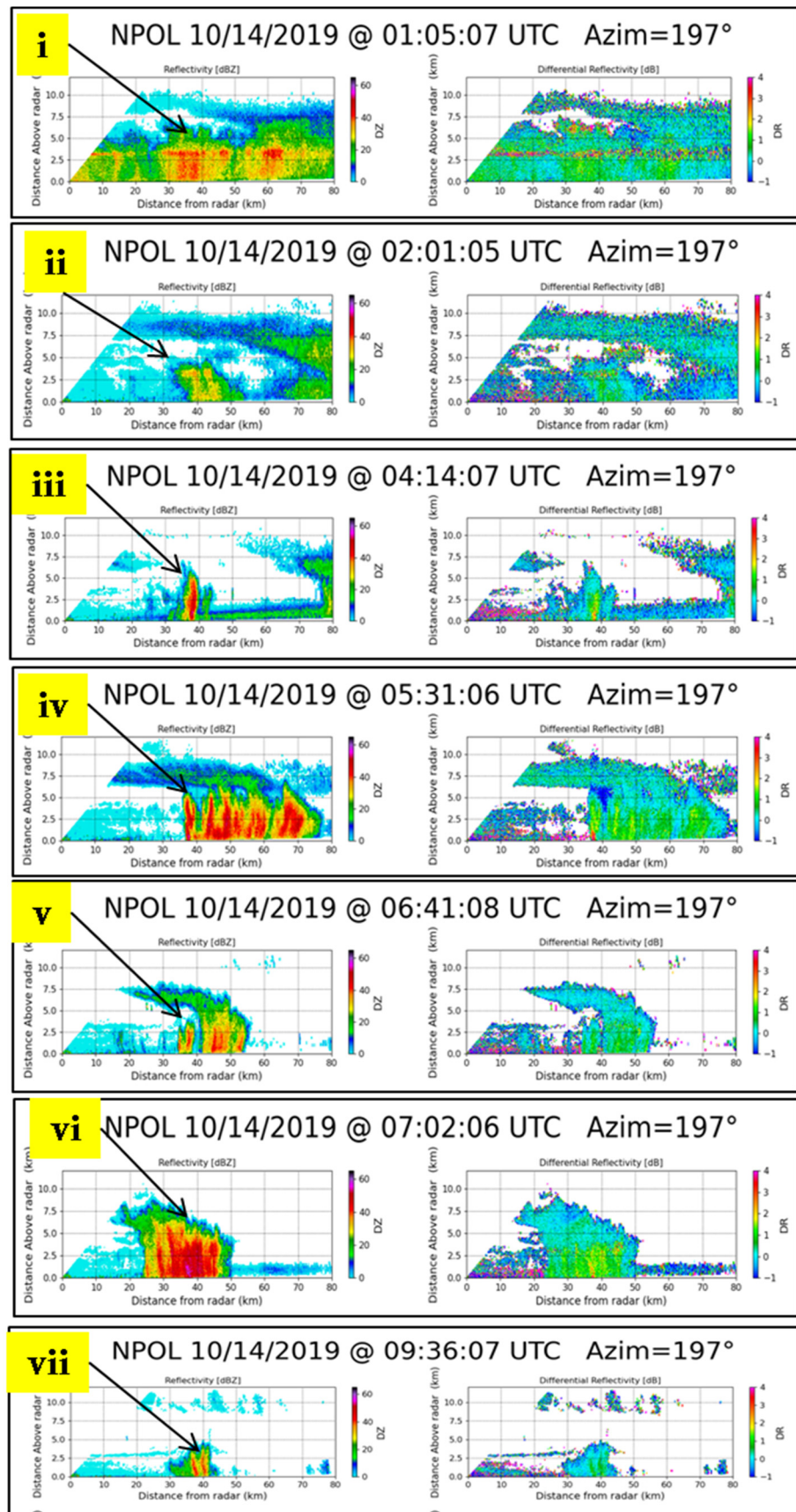


Figure 6. NPOL RHI scans of Z_h and Z_{dr} corresponding to cases (i) to (vii), highlighted in yellow in Figure 5.

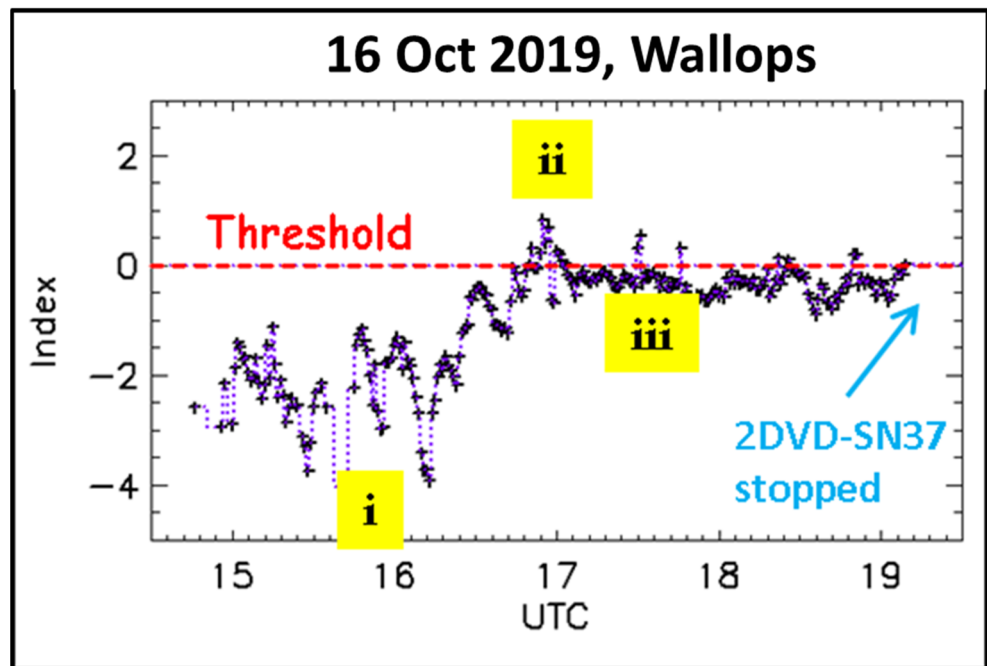


Figure 7. Variation of the “index” parameter with time for the 16 October 2019 event. Cases (i), (ii), and (iii) are marked where the index indicated stratiform, convective, and “mixed” or “uncertain” rain, respectively.

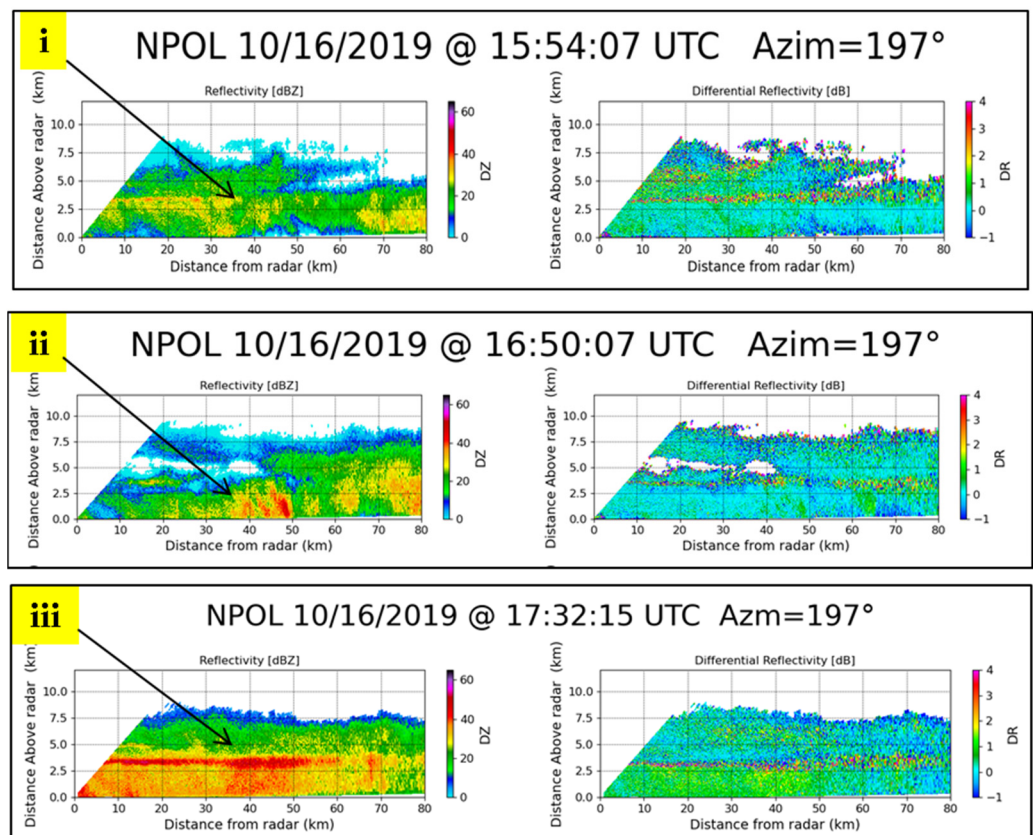


Figure 8. NPOL RHI scans of Z_h and Z_{dr} corresponding to cases (i), (ii), and (iii) highlighted in yellow in Figure 7.

4. Rain-Bands of Hurricane Dorian

This event also lasted for many hours over the Wallops site. The N_w and D_m from the measured 3 min DSDs are shown in Figure 9a,b, and their variation against one another is shown in panel (c) where the colors represent different hours (as shown in the figure). The separation line is shown as dashed black line.

According to the DSD-based classification, much of this event was stratiform rain. This was in agreement with the regular NPOL RHI scans taken throughout the event (not shown here). There are, however, a few points that appear to lie above the black line in panel (c). They are mostly in the time period of 15:00 to 16:00 UTC, and have $D_m > 2$ mm. From panel (b), we see that the points correspond to 15:30 to 16:00 UTC. The index values are shown in panel (d), where slightly positive values can be seen.

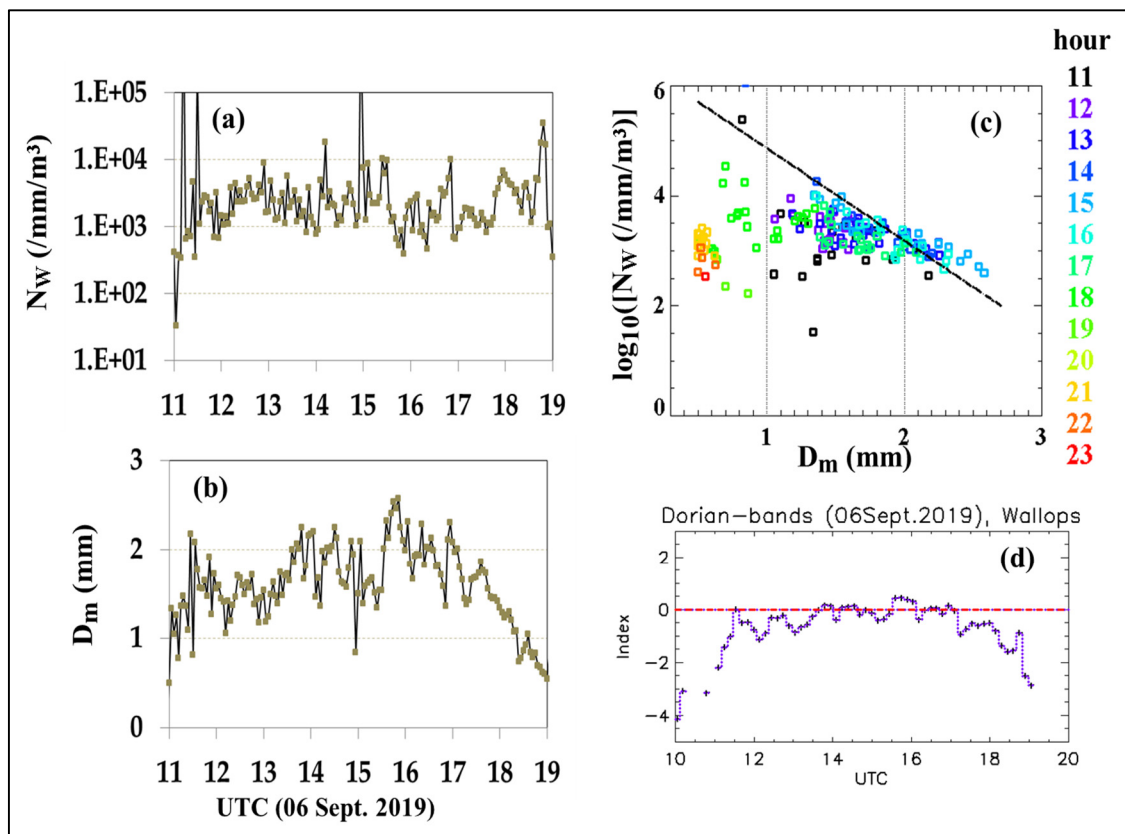


Figure 9. (a) N_w and (b) D_m variation with time from the 3 min composite DSDs; (c) $\log_{10}(N_w)$ versus D_m from the 3 min DSDs for each hour (color-coded), and (d) variation of the convective-stratiform rain index with time.

During this time period, several large drops were recorded by the 2DVD, including a very large (fully melted) drop with D_{eq} of 8 mm. An RHI scan at 15:41 UTC is shown in panels (a) and (b) of Figure 10. The rain type was very definitely stratiform rain, with clearly defined bright-band both in Z_h and Z_{dr} . Panels (c) and (d) show the vertical profiles of Z_h and q_{hv} over and surrounding the disdrometers. Similar to Figure 3e,f, Z_h profiles showed a very clear peak (4 to 4.5 km for this case), and the q_{hv} profiles showed a corresponding dip in the melting layer. Hence for this case, between 15:30 and 16:00 UTC, our DSD-based classification did not correctly identify the rain type. One feature worth noting in the RHI scan is the layer of enhanced Z_{dr} at around 8 km height. This was attributed to the dendritic growth zone, which typically occurs at around -15 °C height [30].

5. Summary

More than 20 h of DSD data from three events in the Delmarva peninsula were tested. The DSD-based classification correctly identified stratiform and convective rain types for all cases throughout all three events, except for a 30 min period during the event relating to Hurricane Dorian rain-bands. This 30 min period was unusual in that there were many large drops, including one with a D_{eq} of 8 mm (fully melted) drop, and yet a clear bright-band was present around the 0 °C isotherm height. However, the bright-band thickness and the dBZ peak were high.

Data and observations from three other locations, i.e., Huntsville, Alabama, and Greeley, Colorado (as well as Ontario, Canada), supported the separation line in the N_w – D_m space. Additionally, in Figure 11 we show the separation line along with some readily available data points from [5]. Based on the location and rain-types (either from radar observations or using the standard deviation of rain rate with time), these data points were classified into: (i) stratiform rain, (ii) tropical-convective, and (iii) continental-convective rain. Their locations, and the mean values of D_m and $\log_{10}(N_w)$, together with the corresponding standard deviations, are presented in Table 1. They are from different continents and have very different climatologies, but even so, our N_w – D_m line seemed to separate the stratiform and convective rain types for all cases.

Finally, in Appendix A, we demonstrate how the N_w – D_m separation technique can be used to identify convective and stratiform rain regions from NPOL radar scans.

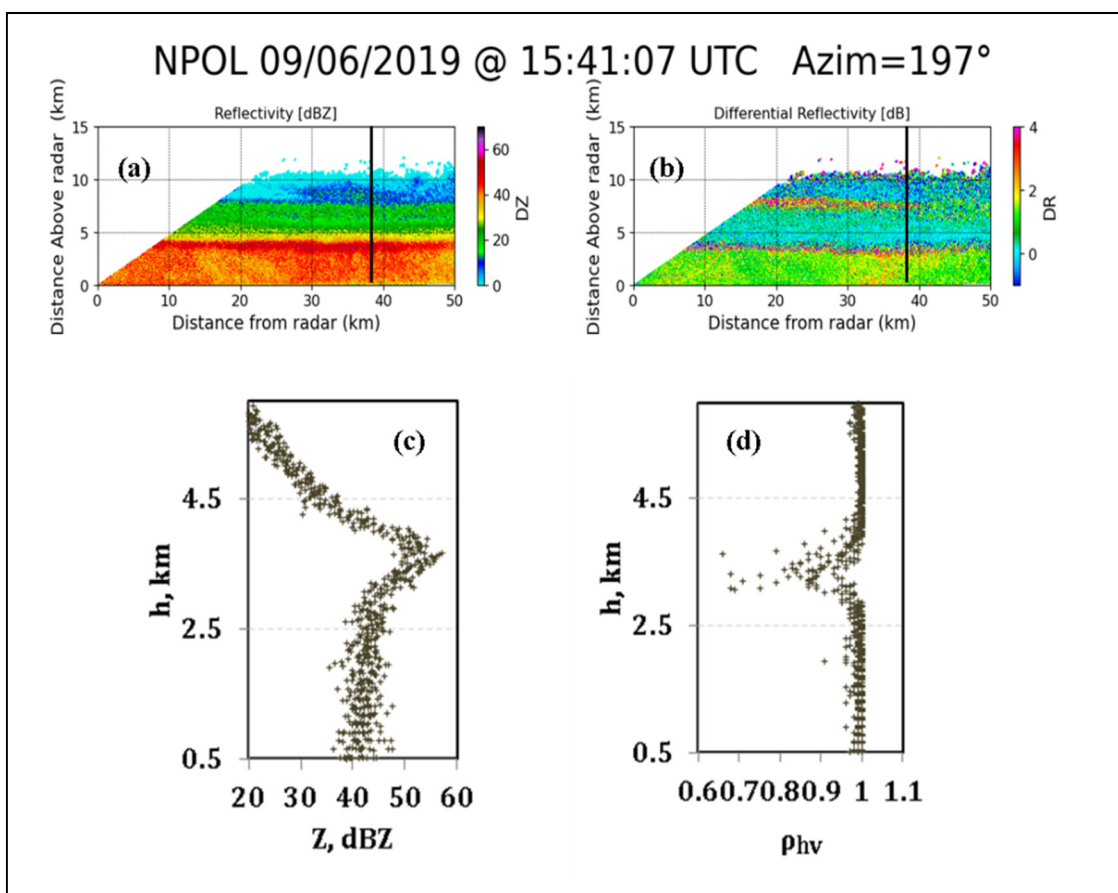


Figure 10. RHI scans of (a) Z_h and (b) Z_{dr} during a stratiform rain event (with thick bright-band) on 6 September 2019, i.e., rain-bands of Dorian storm; (c) and (d): vertical profiles of Z_h and ρ_{hv} , respectively, over the disdrometers (black lines in panels (a) and (b)).

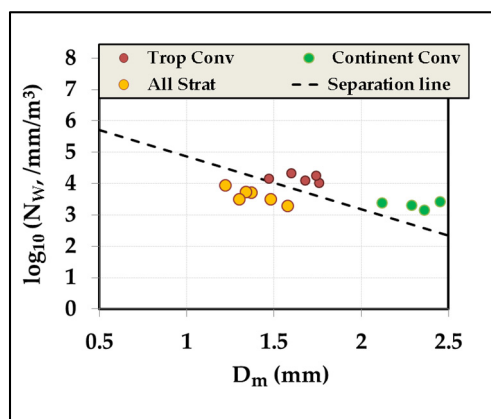


Figure 11. The $\log_{10}(N_w)$ versus D_m for some locations and rain-types from [5], as given in Table 1.

Table 1. Locations and disdrometer types for data points used in Figure 11, along with the mean values of D_m and $\log_{10}(N_w)$, and their corresponding standard deviations.

| | | Site (Disdrometer Type) | $\langle D_m \rangle$ mm | Std dev. of D_m in mm | Log $\langle N_w \rangle$ | Std dev. of log N_w |
|-----------|-------|---|--------------------------|----------------------------|---------------------------|--------------------------|
| Tropical | Conv | Darwin (Joss) | 1.68 | 0.385 | 4.1 | 0.36 |
| | | SCSMX (Joss) | 1.76 | 0.326 | 4.03 | 0.312 |
| | | Papua New Guinea (2DVD) | 1.47 | 0.32 | 4.15 | 0.327 |
| | | Florida (2DVD) | 1.74 | 0.49 | 4.25 | 0.52 |
| | | TOGA-COARE (from airborne data) | 1.6 | 0.34 | 4.33 | 0.4 |
| Continent | Conv | Graz (2DVD) | 2.12 | 0.53 | 3.39 | 0.45 |
| | | Sydney (Joss) | 2.29 | 0.51 | 3.3 | 0.34 |
| | | Arecibo (Joss) | 2.36 | 0.17 | 3.15 | 0.27 |
| | | Colorado (2DVD) | 2.45 | 0.58 | 3.43 | 0.38 |
| All | Strat | Darwin (Joss) | 1.37 | 0.31 | 3.72 | 0.4 |
| | | SCSMX (Joss) | 1.34 | 0.28 | 3.73 | 0.35 |
| | | Papua New Guinea (2DVD) | 1.22 | 0.31 | 3.94 | 0.52 |
| | | Florida (2DVD) | 1.48 | 0.34 | 3.5 | 0.48 |
| | | TOGA-COARE (from airborne data from Testud) | 1.3 | 0.28 | 3.49 | 0.5 |
| | | Colorado (2DVD) | 1.58 | 0.3 | 3.28 | 0.24 |

Note: JOSS: Joss Waldvogel disdrometer; SCSMX: South China Sea Monsoon Experiment; TOGA-COARE: Tropical Ocean–Global Atmosphere–Coupled Ocean Atmosphere Response Experiment.

Author Contributions: Conceptualization, M.T. and V.B.; methodology, investigation, and formal analysis, M.T. and V.B.; data curation, D.M., D.W., and C.P.; writing—original draft preparation, M.T.; writing—review and editing, V.B. and D.W.; supervision, V.B.; resources, D.W. All authors have read and agreed to the published version of the manuscript.

Data Availability Statement: Data can be made available upon request to any of the authors.

Acknowledgments: M.T. received funding to conduct this research from NASA’s Precipitation Measurement Mission via grant award number 80NSSC19K0676. V.B. was funded by the US National Science Foundation under grant AGS190585.

Conflicts of Interest: The authors declare no conflict of interest. The funders had no role in the design of this study; in the collection, analyses, or interpretation of its data; in the writing of this manuscript; or in the decision to publish these results.

Appendix A

The DSD-based separation technique can also be used to identify stratiform and convective rain regions from NPOL radar scans. It entails, as a first step, the estimation of the two DSD parameters needed for the separation, N_w and D_m . Initially, the mass-weighted mean diameter, D_m , is estimated using the S-band Z_{dr} via a two-step procedure that involves an intermediate parameter, D_m' , as defined in [31]. D_m' depends on two (chosen) reference DSD moments. In [32], where X-band polarimetric radar retrievals were successfully carried out, the chosen reference moments were the 3rd and the 6th moments. We used a similar approach here, except the frequency was S-band.

Scattering (T-matrix) calculations using 3 min DSD spectra (from the Greeley and Huntsville campaigns) have been used to derive the retrieval equations. Figure A1 shows the variations of: (a) D_m' with the S-band Z_{dr} , (b) D_m with D_m' , and (c) $N_w/Z_h(\text{linear})$ versus D_m' . The fitted equations are given in each of the panels. These were applied to the radar scans, and the results are shown in Figure A2 for the two cases presented earlier in Figure 2. Panels (a) to (d) correspond to the Dorian rain-band event on 06 September 2019 at 11:29 UTC, and panels (e) to (h) correspond to 14 October 2019 at 05:31 UTC. For both cases, the retrieved N_w and D_m are shown in panels (a), (e), (b), and (f), respectively, and the index values are shown in panels (c) and (g). Only the rain region is shown in all cases, up to 3 km above ground level. Note also for the second event that the radar range goes from 35 km to 60 km, since there was no precipitation at closer range. The retrieved N_w versus D_m from the radar scans (below 3 km height) are shown in panels (d) and (h), with the separation line (in red) overplotted.

The differences between the two events can be clearly observed from Figure A2. N_w shows more uniformity for the stratiform rain event, and D_m shows higher values for some regions in the convective event. The index values are mostly negative for the 06 September 2019 case and mostly positive for the 14 October 2019 case. This not only lends support to the separation method (largely), but also provides general support to our retrieval method for the DSD parameters from the NPOL radar scans. Note also from panels (d) and (h) that most points lie below the red line for the stratiform rain case, except for very low D_m points (which need to be categorized as light rain events and considered separately), while most points lie above the red line for the convective rain case.

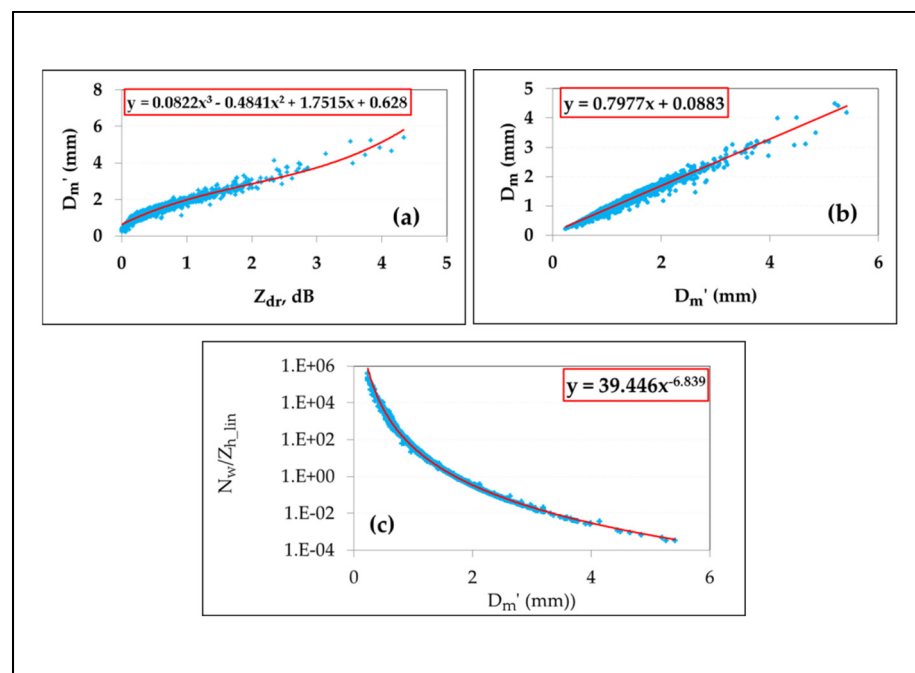


Figure A1. S-band simulation results of (a) D_m' versus Z_{dr} ; (b) D_m with D_m' ; (c) $N_w/Z_h(\text{linear})$ versus D_m' .

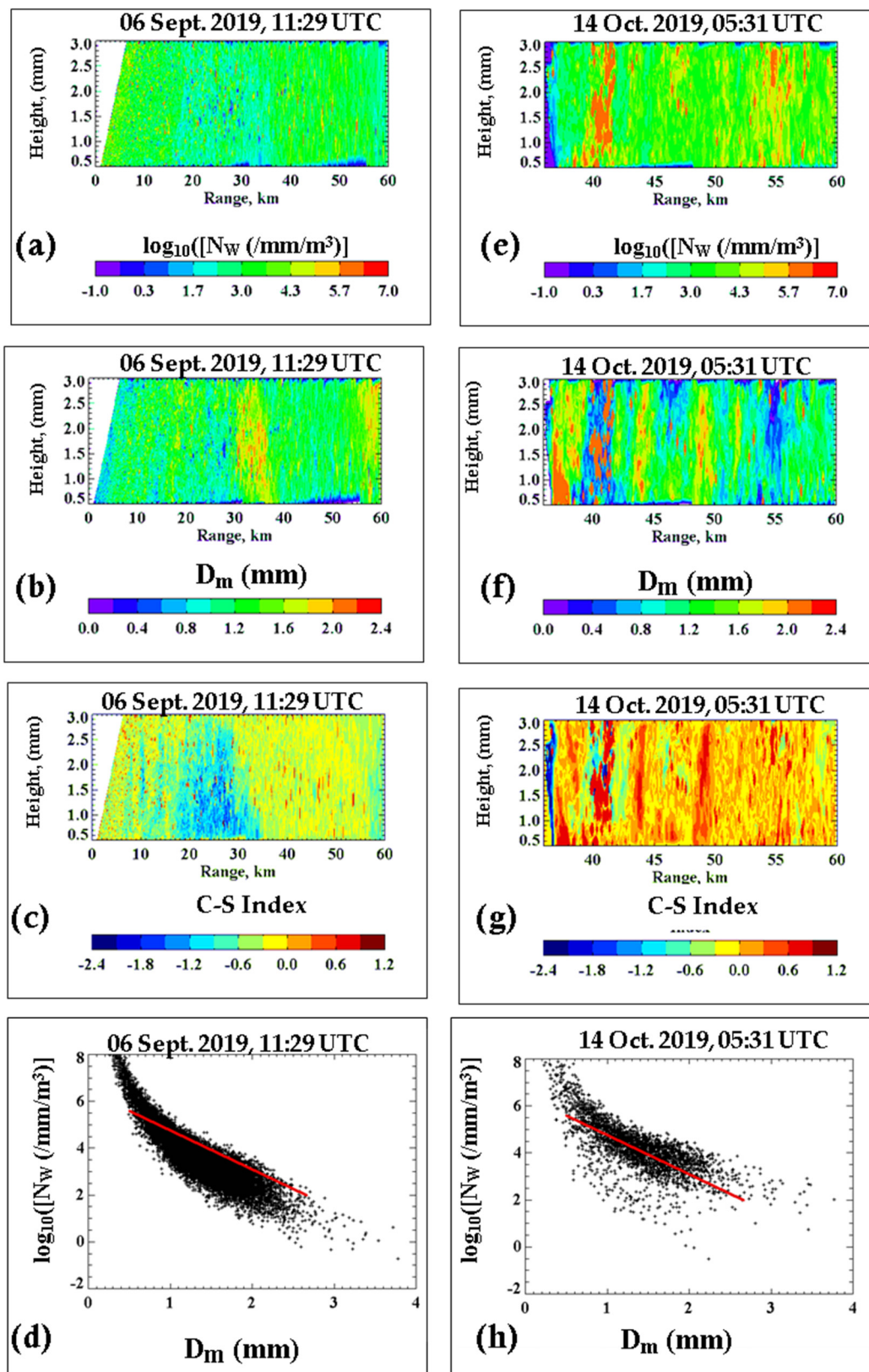


Figure A2. Retrievals from NPOL-RHI scans from the 06 September 2019 event (left panels) and from the 14 October 2019 event (right panels). (a) and (e): The retrieved N_w ; (b) and (f): the retrieved D_m ; (c) and (g): the index values; and (d) and (h): the N_w versus D_m for the two cases.

References

1. Steiner, M.; Houze, R.A.; Yuter, S.E. Climatological Characterization of Three-Dimensional Storm Structure from Operational Radar and Rain Gauge Data. *J. Appl. Meteor.* **1995**, *34*, 1978–2007.
2. Tao, W.; Iguchi, T.; Lang, S. Expanding the Goddard CSH Algorithm for GPM: New Extratropical Retrievals. *J. Appl. Meteor. Climatol.* **2019**, *58*, 921–946.
3. Houze, R.A., Jr. *Cloud Dynamics*; Academic Press: Cambridge, MA, USA, 1993; 573p.
4. Tokay, A.; Short, D.A. Evidence from Tropical Raindrop Spectra of the Origin of Rain from Stratiform versus Convective Clouds. *J. Appl. Meteor.* **1996**, *35*, 355–371.
5. Bringi, V.N.; Chandrasekar, V.; Hubbert, J.; Gorgucci, E.; Randeu, W.L.; Schoenhuber, M. Raindrop Size Distribution in Different Climatic Regimes from Disdrometer and Dual-Polarized Radar Analysis. *J. Atmos. Sci.* **2003**, *60*, 354–365.
6. Thompson, E.J.; Rutledge, S.A.; Dolan, B.; Thurai, M. Drop Size Distributions and Radar Observations of Convective and Stratiform Rain over the Equatorial Indian and West Pacific Oceans. *J. Atmos. Sci.* **2015**, *72*, 4091–4125.
7. Atlas, D.; Ulbrich, C.W.; Marks, F.D., Jr.; Black, R.A.; Amitai, E.; Willis, P.T.; Samsur, C.E. Partitioning tropical oceanic convective and stratiform rains by draft strength. *J. Geophys. Res.* **2000**, *105*, 2259–2267.
8. Testud, J.; Oury, S.; Black, R.A.; Amayenc, P.; Dou, X. The concept of “normalized” distribution to describe raindrop spectra: A tool for cloud physics and cloud remote sensing. *J. Appl. Meteorol.* **2001**, *40*, 1118–1140.
9. Ulbrich, C.W.; Atlas, D. On the separation of tropical convective and stratiform rains. *J. Appl. Meteor.* **2002**, *41*, 188–195.
10. Yuter, S.E.; Houze, R.A., Jr. Measurements of raindrop size distributions over the Pacific warm pool and implications for Z–R relations. *J. Appl. Meteor.* **1997**, *36*, 847–867.
11. Bukovcic, P.; Zrnica, D.; Zhang, G. Convective–stratiform separation using video disdrometer observations in central Oklahoma—the Bayesian approach. *Atmos. Res.* **2009**, *155*, 176–191.
12. Schoenhuber, M.; Lammer, G.; Randeu, W.L. One decade of imaging precipitation measurement by 2D-video-distrometer. *Adv. Geosci.* **2007**, *10*, 85–90.
13. Schönhuber, M.; Lammer, G.; Randeu, W.L. The 2D-Video-Distrometer. In *Precipitation: Advances in Measurement, Estimation and Prediction*; Michaelides, S., Ed.; Springer: Berlin/Heidelberg, Germany, 2008; pp. 3–31, ISBN 978-3-540-77654-3.
14. Bringi, V.N.; Williams, C.R.; Thurai, M.; May, P.T. Using dual-polarized radar and dual-frequency profiler for DSD characterization: A case study from Darwin, Australia. *J. Atmos. Oceanic Technol.* **2009**, *26*, 2107–2122.
15. Thurai, M.; Bringi, V.N.; May, P.T. CPOL radar-derived drop size distribution statistics of stratiform and convective rain for two regimes in Darwin, Australia. *J. Atmos. Oceanic Technol.* **2010**, *27*, 932–942.
16. Thurai, M.; Gatlin, P.N.; Bringi, V.N. Separating stratiform and convective rain types based on the drop size distribution characteristics using 2D video disdrometer data. *Atmos. Res.* **2016**, *169 Pt B*, 416–423.
17. Thurai, M.; Kennedy, P.; Dolan, B.; Bringi, V.N. Testing the DSD-Based Stratiform–Convective Rain Separation for Ten Events in Greeley, Colorado. In Proceedings of the 38th Conference on Radar Meteorology, Chicago, IL, USA, 1 September 2017; p. 24.
18. Knollenberg, R. The optical array: An alternative to scattering or extinction for airborne particle size determination. *J. Appl. Meteorol.* **1970**, *9*, 86–103.
19. Baumgardner, D.; Kok, G.; Dawson, W.; O’Connor, D.; Newton, R. A new ground-based precipitation spectrometer: The Meteorological Particle Sensor (MPS). In Proceedings of the 11th Conference on Cloud Physics, Ogden, UT, USA, 3–7 June 2002.
20. Bringi, V.N.; Thurai, M.; Baumgardner, D. Raindrop fall velocities from an optical array probe and 2-D video disdrometer. *Atmos. Meas. Tech.* **2018**, *11*, 1377–1384.
21. Bringi, V.N.; Hoferer, R.; Brunkow, D.A.; Schwerdtfeger, R.; Chandrasekar, V.; Rutledge, S.A.; George, J.; Kennedy, P.C. Design and Performance Characteristics of the New 8.5-m Dual-Offset Gregorian Antenna for the CSU–CHILL Radar. *J. Atmos. Oceanic Technol.* **2011**, *28*, 907–920.
22. Skofronick-Jackson, G.; Petersen, W.A.; Berg, W.; Kidd, C.; Stocker, E.F.; Kirschbaum, D.B.; Kakar, R.; Braun, S.A.; Huffman, G.J.; Iguchi, T.; et al. The Global Precipitation Measurement (GPM) Mission for science and society. *Bull. Am. Meteorol. Soc.* **2016**, *98*, 1679–1696.
23. Tokay, A.; Bashor, P.G.; McDowell, V.L. Comparison of Rain Gauge Measurements in the Mid-Atlantic Region. *J. Hydrometeorol.* **2010**, *11*, 553–565.
24. OTT Hydromet GmbH. Operating Instructions: OTT Pluvio2 Precipitation Gauge. *OTT Hydromet* **2010**, *60*. Available online: <http://www.ott.com/en-us/products/download/operating-instructions-precipitation-gauge-ott-pluvio2/> Accessed Jan 2021.
25. Rasmussen, R.; Baker, B.; Kochendorfer, J.; Meyers, T.; Landolt, S.; Fischer, A.P.; Black, J.; Thériault, J.M.; Kucera, P.; Gochis, D.; Smith, C.; Nitu, R.; Hall, M.; Ikeda, K.; Gutmann, E. How Well Are We Measuring Snow: The NOAA/FAA/NCAR Winter Precipitation Test Bed. *Bull. Amer. Meteor. Soc.* **2012**, *93*, 811–829.
26. Raupach, T.H.; Thurai, M.; Bringi, V.N.; Berne, A. Reconstructing the Drizzle Mode of the Raindrop Size Distribution Using Double-Moment Normalization. *J. Appl. Meteor.* **2019**, *58*, 145–164.
27. Wolff, D.B.D.A. Marks, and W.A. Petersen, 2015: General Application of the Relative Calibration Adjustment (RCA) Technique for Monitoring and Correcting Radar Reflectivity Calibration. *J. Atmos. Oceanic Technol.* **2015**, *32*, 496–506.
28. Thurai, M.; Bringi, V.N.; Wolff, D.B.; Marks, D.A.; Pabla, C.S. Drop Size Distribution Measurements in Outer Rainbands of Hurricane Dorian at the NASA Wallops Precipitation-Research Facility. *Atmosphere* **2020**, *11*, 578.

-
29. Bringi, V.; Seifert, A.; Wu, W.; Thurai, M.; Huang, G.-J.; Siewert, C. Hurricane Dorian Outer Rain Band Observations and 1D Particle Model Simulations: A Case Study. *Atmosphere* **2020**, *11*, 879.
 30. Kennedy, P.C.; Rutledge, S.A. S-Band Dual-Polarization Radar Observations of Winter Storms. *J. Appl. Meteor. Climatol.* **2011**, *50*, 844–858.
 31. Lee, G.; Zawadzki, I.; Szyrmer, W.; Sempere-Torres, D.; Uijlenhoet, R. A General Approach to Double-Moment Normalization of Drop Size Distributions. *J. Appl. Meteor.* **2004**, *43*, 264–281.
 32. Bringi, V.N.; Mishra, K.V.; Thurai, M.; Kennedy, P.C.; Raupach, T.H. Retrieval of lower-order moments of the drop size distribution using CSU-CHILL X-band polarimetric radar: A case study. *Atmos. Meas. Tech.* **2020**, *13*, 4727–4750.